9-1-2007

Gas Feedback on Stellar Bar Evolution

Ingo Berentzen
University of Kentucky, iberent@pa.uky.edu

Isaac Shlosman
University of Kentucky, isaac.shlosman@uky.edu

Inma Martinez-Valpuesta
University of Kentucky, martinez@pa.uky.edu

Clayton Heller
Georgia Southern University, cheller@georgiasouthern.edu

The Astrophysical Journal, 666:189–200, 2007 September 1

GAS FEEDBACK ON STELLAR BAR EVOLUTION

Ingo Berentzen,[1] Isaac Shlosman, and Inma Martinez-Valpuesta[2,3]
Department of Physics and Astronomy, University of Kentucky, Lexington, KY 40506-0055;
iberent@pa.uky.edu, shlosman@pa.uky.edu, martinez@pa.uky.edu

and

Clayton H. Heller
Department of Physics, Georgia Southern University, Statesboro, GA 30460; cheller@georgiasouthern.edu
Received 2007 February 28; accepted 2007 May 22

ABSTRACT

We analyze evolution of live disk-halo systems with gas fractions, $f_{\rm gas} \leq 8\%$ of the disk mass, for 5 Gyr. Specifically, we have addressed the issue of angular momentum (J) transfer from the gas to the stellar bar and its effect on the bar. We find that the bar weakening, reported in the literature, is not related to the gas, but is caused by the vertical buckling instability in the gas-poor disks and by a steep stellar heating by the central mass concentration (CMC) in the gas-rich disks. However, the gas has a profound effect on the onset of the buckling: larger $f_{\rm gas}$ brings it forth due to the more massive CMCs. The former process leads to the well-known formation of the boxy/peanut-shaped bulges, while the latter results in the formation of more elliptical bulges, for larger $f_{\rm gas}$. The subsequent secular bar evolution differs: the gas-poor models exhibit a growing bar while gas-rich models show a declining bar whose vertical swelling is driven by a resonance heating. The borderline between the gas-poor and gas-rich models is model-dependent and will be affected by processes such as star formation and stellar feedback. The overall effect of the gas on the bar is not in a direct J transfer to the stars, but in the loss of J by the gas and the gas influx to the center. A more massive CMC damps the bar buckling and depopulates orbits responsible for the appearance of boxy/peanut-shaped bulges. The combined action of resonant and nonresonant processes in gas-poor and gas-rich disks leads to a converging evolution in the vertical extent of the bar and its stellar dispersion velocities, and to a diverging evolution in the bulge properties.

Subject headings: galaxies: bulges — galaxies: evolution — galaxies: formation — galaxies: halos — galaxies: kinematics and dynamics — galaxies: structure

Online material: color figures

1. INTRODUCTION

Galactic bars break the axial symmetry of rotating disks in the most profound way because they are sufficiently massive—thus being of a paramount importance to the short- and long-term galaxy evolution. However, various processes associated with bars are still poorly understood. Barred galaxies consist of stellar disks embedded in the dark matter (DM) halos with an admixture of gas. This gas is deprived of the rotational support by the bar and is channeled toward the central regions of a few $\times 100$ pc to 1 kpc, accumulating there in the form of the central mass concentration (CMC), which includes gas, stars, and a certain amount of the DM, and typically harbors the central supermassive black hole (SBH). Our main goal is to analyze the changes in the stellar bar as a result of this process—in other words to study the gas feedback on the bar evolution.

In self-gravitating systems with a dynamically significant rotation, any substantial departure from axial symmetry is destined to speed up the evolution, leading to mass and angular momentum redistribution in the system. While the role of the angular momentum in this process has been emphasized already by Lynden-Bell & Kalnajs (1972), the efficiency of this transport and dependence on various parameters is still under investigation (e.g., Athanassoula 2003). Tremaine & Weinberg (1984) and Weinberg (1985) have estimated that the bar should lose most of its momentum to the surrounding DM halo in a few rotations ($\sim$1 Gyr); this was not supported by subsequent numerical simulations (Sellwood 2006), but the overall trend, that the angular momentum flows from the inner, bar-unstable disk to the outer disk and to the halo, has been confirmed.

Our view on the role of a DM halo in disk galaxy evolution has changed dramatically over the last few years—from the original claim that it damps the bar instability (e.g., Ostriker & Peebles 1973), to recent results that more massive halos grow larger bars (e.g., Athanassoula & Misiriotis 2002). It is a common wisdom today that bars on all scales redistribute mass and angular momentum in the main body of the galaxy and alter the radial profiles of gas, stars, and DM densities. In the long run, the DM halos serve as a sink for the angular momentum from the disk and this process is mediated by the bars.

Disk galaxies possess various amounts of a cold gas, typically $<10\%$ of the disk mass, and probably have been more gas-rich in the past. However, the ability of the gas to influence the galactic dynamics of the parent object extends well beyond its mass fraction. The gas dissipates and therefore can form bound massive accumulations even in excess of $10^7\,M_\odot$. In this sense the gas can be more clumpy than a collisionless matter, either stellar or DM. This leads to a number of dynamical consequences, more importantly to a dynamical friction and to scattering and randomizing of stellar and DM particle orbits (Shlosman & Noguchi 1993). The angular momentum redistribution in numerical simulations with gas has been examined by Berentzen al. (1998, 2004).

Furthermore, the gas bears similar amounts of a *specific* angular momentum with stars in the cold disk prior to the bar instability. Because of its viscosity, the gas responds to a barlike

[1] Current address: Astronomisches Rechen-Institut, Zentrum für Astronomie, D-69120 Heidelberg, Germany.
[2] Gruber Foundation Fellow at OAMP, 13004 Marseille, France.
[3] Current address: Instituto de Astrofisica de Canarias, E-38200 La Laguna, Tenerife, Spain.

perturbation with a phase shift, compared to the stellar response. This leads to streamline intersections and to shocks downstream from the bar major axis. Resulting leading dust lanes delineate the underlying shocks and associated density enhancements (e.g., Athanassoula 1992). The gravitational torques from the bar extract the angular momentum from the gas and transfer it to the underlying stellar (and DM) component that lags behind the gas. These torques depend on the shift in the position angle between the gas and stellar distributions in the bar,

$$\text{torque} = -\left[\int_0^{2\pi}\int_0^{\infty} \Sigma^a(r,\ \phi)\frac{\partial \Phi^a_{\rm gas}(r,\ \phi)}{\partial \phi}\right] r\, dr\, d\phi, \quad (1)$$

where only the *asymmetric* part of the gas gravitational potential $\Phi^a_{\rm gas}$, which acts on the segment dr of the *asymmetric* stellar density distribution $\Sigma^a(r,\ \phi)$ in the cylindrical system of coordinates r, ϕ, will make a nonzero contribution.

As a result, the gas falls toward the central kpc where the bar potential is again more axisymmetric and the resulting shock focusing injects the gas onto the weakly elliptical orbits in situ, forming nuclear rings. These rings are ubiquitous in barred galaxies (Buta & Combes 1996; Knapen 2005), but their subsequent evolution can differ (Knapen et al. 1995; Heller & Shlosman 1996; Heller et al. 2001; Shlosman & Heller 2002; Englmaier & Shlosman 2004). The ultimate fate of the inflowing gas is debatable, but there is a strong theoretical and observational evidence that some of this gas can reach deep inside the central region and fuel the nuclear star formation and the accretion processes onto the central SBH as a result of gravitational instabilities in the gas itself (e.g., Shlosman et al. 1989, 1990; Ishizuki et al. 1990; Kenney et al. 1992; Forbes et al. 1994; Knapen et al. 1995; Maiolino et al. 2000; Jogee et al. 2002; Shlosman 2005; Jogee 2006), and contribute to the formation of the BH itself (Begelman et al. 2006; Heller et al. 2007).

Whether the inflowing gas fuels the central SBH, or contributes to the buildup of stellar bulges (Kormendy & Kennicutt 2004 and references therein), the growing CMC in barred galaxies has been reported to have a strong effect on the stellar bar. Hasan & Norman (1990), Friedli (1994), Norman et al. (1996), Berentzen et al. (1998), Shen & Sellwood (2004), and others have observed that the bar dissolves only when massive and compact CMCs form—a process that is affected by the bar structure and its host DM halo (Athanassoula et al. 2005). Such extreme CMCs can be represented only by the SBHs. However, the required SBH mass of a few percent of the disk mass is more than a factor of 10 larger than the SBH masses found in disk galaxies (e.g., Ferrarese & Ford 2005). Hence the stellar bars are much more resilient than previously envisioned.

Furthermore, Bournaud et al. (2005) have argued, based on numerical simulations of 7.25% gas-rich disks embedded in *rigid* halos, that the gas is able to weaken the stellar bars dramatically, even *before* the CMC is in place; the reason for this is the transfer of angular momentum from the gas to the bar. The combination of angular momentum transfer to the stars and the subsequent buildup of the CMC destroys the bar over the timescale as short as 1.4 Gyr—claimed by Bournaud et al.

Here we analyze the bar evolution for various gas fractions in the disk and allow for the growth of the CMC and SBH. Unlike Bournaud et al. (2005), we use a disk immersed in the live DM halo. In addition to the standard model, we supplement our analysis with a number of test models. We limit the discussion to 5 Gyr of bar evolution in order to make a direct comparison with Bournaud et al. This paper is structured as follows. Section 2 describes our numerical tools and the initial conditions used in this work. Section 3 provides the results and § 4 presents a number of test models. We conclude with the discussion in § 5.

TABLE 1
G0: Standard Model Parameters

Parameter	Stellar Disk	DM Halo	SBH
Radial scale length (kpc)	2.85	...	...
Vertical scale length (kpc)	0.2	...	...
Total mass ($M_\odot$)	0.58×10^{11}	1.33×10^{11}	0
Mass (<10 kpc) ($M_\odot$)	0.5×10^{11}	0.5×10^{11}	0
Gas fraction ($f_{\rm gas}$)	0	0	...

2. NUMERICAL METHOD AND INITIAL CONDITIONS

We use the updated hybrid N-body and smooth particle hydrodynamics (SPH) code of Heller & Shlosman (1994). The version FTM-4.4 of the code uses the FalcON force solver of Dehnen (2002)—a tree code with mutual cell-cell interactions and complexity $O(N)$. It conserves the momentum exactly and is about 10 times faster than the optimally coded Barnes & Hut (1986) tree code. We use a constant gravitational softening of 160 pc for the gas and for the collisionless particles. The amount of DM particles is $N_{\rm DM} = 1.2 \times 10^5$, stellar particles $N_* = 3.6 \times 10^5$, and gas $N_{\rm gas} = 4 \times 10^4$. The DM particle mass is $1.1 \times 10^6\ M_\odot$, the stellar particle is $1.5 \times 10^5\ M_\odot$, and the gas particle is $1.2 \times 10^5\ M_\odot$ for the gas fraction $f_{\rm gas} = 8\%$ of the disk mass. Models with a much larger number of the disk and DM particles, making DM/stellar mass ratio per particle $\sim$1, did not change the evolution over the run times of our models. The energy and angular momentum conservation in the pure collisionless models is better than 0.15% and 0.02%, correspondingly.

For models with SBHs, the central SBH evolution is given by a single stellar particle with initially a small "seed" mass of $10^5\ M_\odot$. It is nailed to the position of the center-of-mass (CoM) of the system at $\tau = 0$ and has a fixed gravitational softening $\epsilon_\bullet =$ 160 pc (a Plummer sphere with a characteristic $r_0 = 160$ pc), except in one model (G0BH80; see Table 2) where $\epsilon_\bullet = 80$ pc. The CoMs of the disk and the halo stay within $\sim$50 pc from the SBH, damping each others motions. We find no differences in the behavior of the CoMs in the models with and without the gas. The accretion radius of the SBH is taken as $R_{\rm acc} = 40$ pc. Particles that are found within this radius *and* that are bound to the SBH are extracted from the simulations and their mass is added to the SBH. The requirement for a small time step near the CMC and the central SBH are satisfied by the hierarchical time steps in the FTM code. We typically use between nine and twelve time bins, each differing by a factor of 2.

The initial conditions (see Table 1) have been obtained iteratively from Fall & Efstathiou (1980) to assemble disk and halo particles in a virial equilibrium (see Heller & Shlosman 1994 for more details). The halo has been relaxed in the frozen disk potential for $\Delta\tau \sim 2.4$ Gyr. The disk is axisymmetric with the Toomre's parameter $Q = 1.5$ for the stars only, and the halo-to-disk mass ratio is $\sim$1 within $R = 10$ kpc, at the start of the simulations. Other values of Q are used as well, and the asymmetric drift is accounted for. When the gas is added to the disk, the total disk mass is kept unchanged. We use the isothermal equation of state (EOS) with the temperature of $T = 10^4$ K but have run also models with the adiabatic EOS; no differences have been detected. The gas has the stellar radial distribution initially; vertically it is in a hydrostatic equilibrium. The pure collisionless model parameters are listed in Table 1, and all the models with gas and additional test models are listed in Table 2. Overall, our initial conditions are

TABLE 2

List of Models

Model (1)	f_{gas} (%) (2)	SBH Properties (3)	Q (4)	Main Figures (5)	Notes (6)
Standard model:					
G0	0	...	1.5	1*a*, 1*b*	Standard model: DM + stellar disk
Models with gas:					
G05	0.5	...	1.5	1*a*, 1*b*, 2	Standard model with 0.5% gas
G2	2	...	1.5	1*a*, 1*b*, 2	As G05 with 2% gas
G4	4	...	1.5	1*a*, 1*b*, 2	As G05 with 4% gas
G6	6	...	1.5	1*a*, 1*b*, 2	As G05 with 6% gas
G8	8	...	1.5	1*a*, 1*b*, 2	As G05 with 8% gas
Models with gas and growing SBH:					
G05BH	0.5	Growing	1.5	1*a*, 1*b*, 3	As G05 but with a growing SBH
G2BH	2	Growing	1.5	1*a*, 1*b*, 3	As G2 but with a growing SBH
G4BH	4	Growing	1.5	1*a*, 1*b*, 3	As G4 but with a growing SBH
G6BH	6	Growing	1.5	1*a*, 1*b*, 3	As G6 but with a growing SBH
G8BH	8	Growing	1.5	1*a*, 1*b*, 3	As G8 but with a growing SBH
Models with gas torques removed:					
G8-25T	8	Growing	1.5	4	25% gas torques removed
G8-50T	8	Growing	1.5	4	50% gas torques removed
G8-75T	8	Growing	1.5	4	75% gas torques removed
G8-100T	8	Growing	1.5	4	100% gas torques removed
Model with "quasi-exact" gas force:					
G0GT	...	...	1.5	5	No gas, adding "quasi-exact" gas force field in form of an external potential from G8BH
Models using G8BH model:					
G0BH	0	Growing	1.5	6	Using G8BH model for the SBH growth
G0BH250	0	Growing	1.5	6	Using G8BH model for the SBH growth and gas inside r_0 = 250 pc added to the SBH
G0BH80	0	Growing	1.5	7	Using G8BH model: SBH mass including gas within 250 pc. The only model that has $\epsilon_\bullet$ = 80 pc.
G0BH750	0	Growing	1.5	7	Using G8BH for the SBH and gas (Plummer sphere within r_0 = 750 pc) growth
Models with Q = 1.8:					
G0-Q18	0	...	1.8	8	As G0 but with Q = 1.8
G8BH-Q18	8	Growing	1.8	8	As G8BH but with Q = 1.8

Notes.—Col. (1): Model type (see text). Col. (2): Gas fraction (%) of the disk mass. Col. (3): "Growing" refers to growing the BH from a seed value of $10^5\,M_\odot$. Col. (4): Initial value of Q parameter. Col. (5): Main figure(s) introducing this model. Col. (6): Comments.

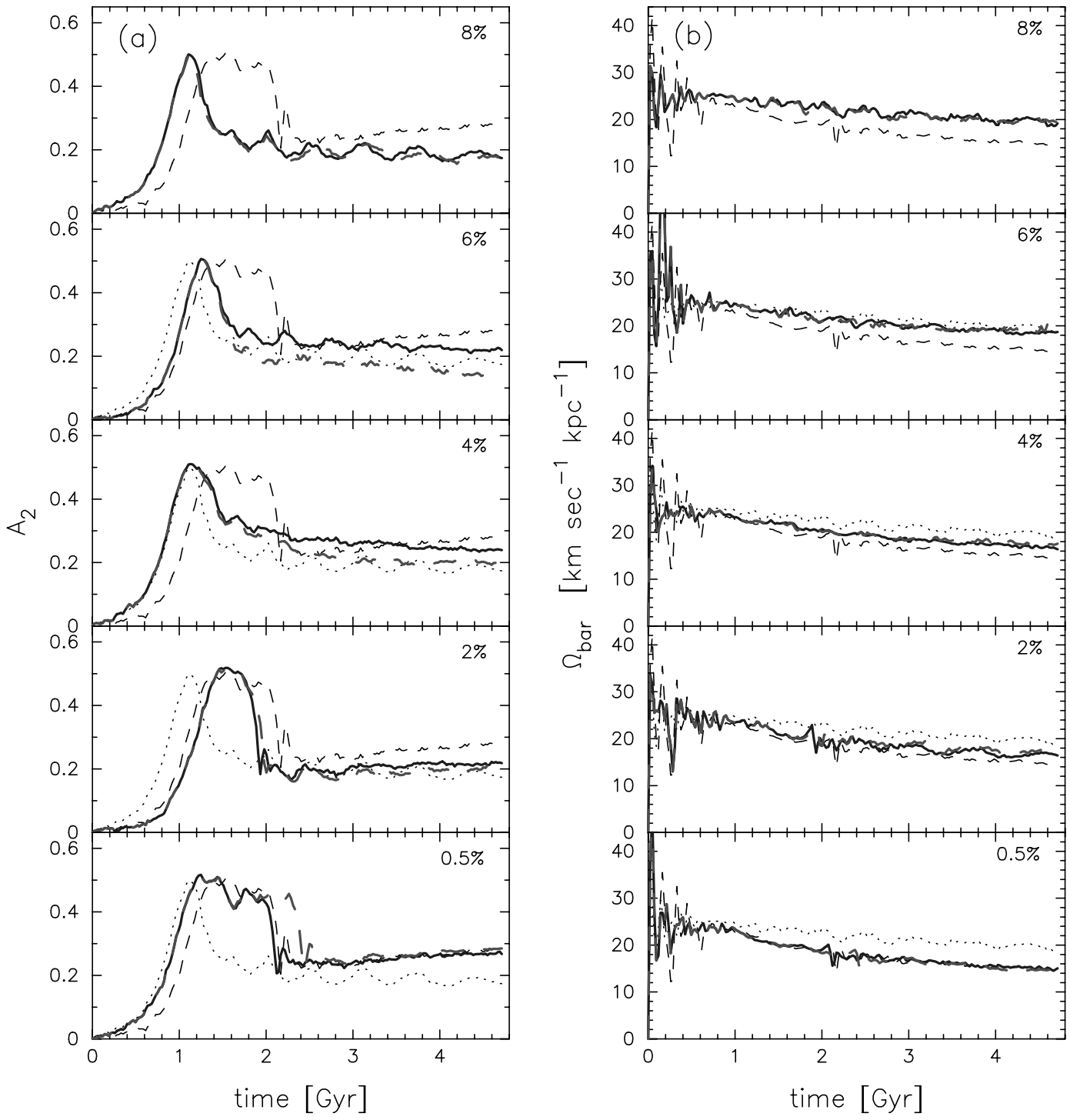

FIG. 1.—Evolution of (*a*) stellar bar amplitude A_2 and (*b*) the bar pattern speed Ω_{bar} (in km s^{-1} kpc^{-1}) given by the $m = 2$ mode in models (*from bottom to top*) G05–G8 (*solid lines*), with various f_{gas}, superposed on models G05BH–G8BH (*long-dashed lines*) with a growing SBH, and on the collisionless model G0 (*short-dashed line*) over the first 5 Gyr. For a comparison, we also display model G8 (*dotted lines*). [*See the electronic edition of the Journal for a color version of this figure.*]

identical to those used by Berentzen et al. (1998), but the numerical resolution in the current models is much superior. This allows us to compare the models and be guided by the Berentzen et al. nonlinear orbit analysis and their usage of the Poincaré sections in dissecting the models.

3. RESULTS: VARYING THE GAS FRACTION

Our benchmark model G0 is a pure collisionless (DM+stars) model that shows a rapidly growing stellar bar whose $m = 2$ normalized amplitude A_2 of the stellar component saturates at $\tau \sim 1.2$ Gyr. We define A_2 within a cylindrical region of 0 kpc $\leq r \leq$ 7.5 kpc and $|z| \leq 1$ kpc, so it encompasses the modeled stellar bars at nearly all times, and normalize it by the amplitude of the $m = 0$ term. After the extended plateau of about 0.9 Gyr, this amplitude drops sharply to about $A_2 \sim 0.2$. The following evolution of the bar is that of a gradual strengthening (Fig. 1*a*).

Models with $f_{gas} = 0.5\%$–8% gas, G05–G8 (Fig. 1*a*), without the central BH, show a rise and drop in bar strength similar to that

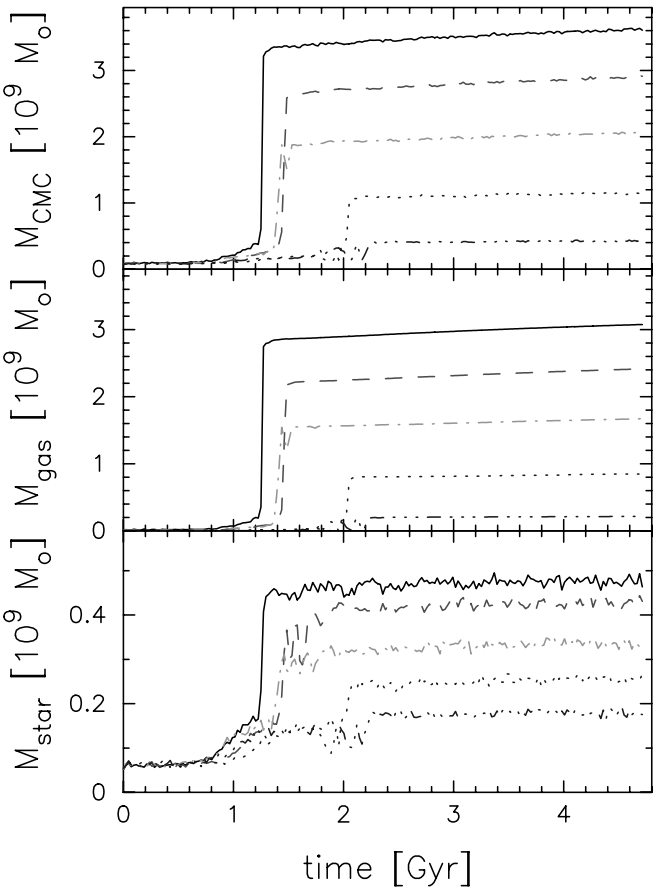

FIG. 2.—Growth of the CMC in models G05–G8 models within the central 250 pc. *Top*: Total (CMC) mass within this radius. *Middle*: Gas mass. *Bottom*: Stellar mass. The lines are as follows: G05 (*dash–triple-dotted lines*), G2 (*dotted lines*), G4 (*dash-dotted lines*), G6 (*dashed lines*), and G8 (*solid lines*). [*See the electronic edition of the Journal for a color version of this figure.*]

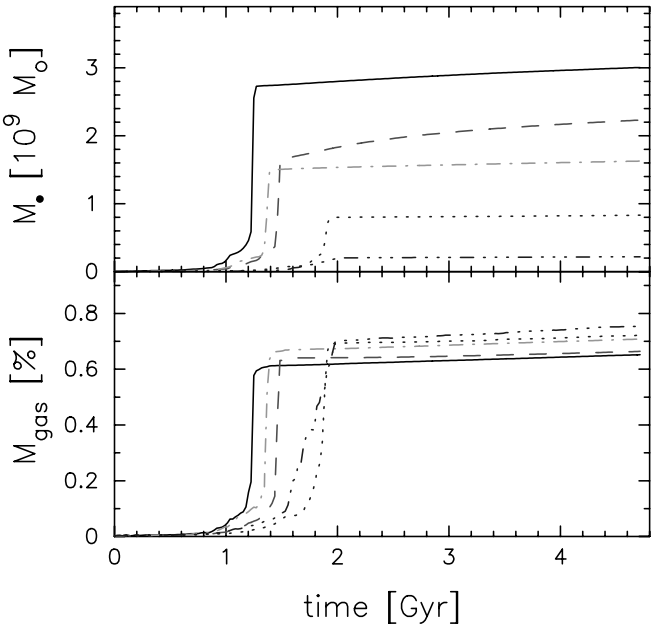

FIG. 3.—Growth of the central BH (*top panel*) in the G05BH–G8BH models, and evolution of the gas fraction of the total CMC mass within the central 250 pc (*bottom panel*). The mass of the BH is counted as contributing to the gas mass. The colors are G05BH (*dotted line*), G2BH (*dash–triple-dotted line*), G4BH (*dash-dotted line*), G6BH (*dashed line*) and G8BH (*solid line*). [*See the electronic edition of the Journal for a color version of this figure.*]

of G0. The main differences appear to be the existence of an extended *plateau* before the drop in A_2, which gradually disappears in models with larger gas fraction, for $\gtrsim$4%, and the maximum in A_2, which is reached slightly earlier for these models. The behavior of A_2 near its maximum changes from G05 to G8 gradually; in the gas-poor models the bar evolution converges to that in G0. Following the large drop, A_2 changes little over the time of the simulations: G0–G2 show a slight increase while G4–G8 models show a slight decrease. Here we focus on the sharp drops in A_2 that are visible in all models.

The bar pattern speeds, Ω_{bar}, are shown in Figure 1*b*. Models with larger f_{gas} slow down more gradually than the gas-poor models, by about 30%. There is also a substantial difference between the behavior of the corotation (CR) radius in gas-rich and gas-poor models. In G0, the CR increases from $\sim$9 to 14 kpc, while that of the G8 model stays flat initially and then increases negligibly to 10 kpc over the simulation time of 5 Gyr.

The CMCs that correspond to a total mass accumulation within the central 250 pc, as well as their gaseous and stellar components, for models G05–G8, are displayed in Figure 2. The pure stellar model G0 does not grow a visible CMC, while other models grow it during 0.2–1.5 Gyr, with the longest timescale corresponding to the most gas-poor models. The growth period can be roughly divided into the initial shallow growth—this is more prolonged for models with lower f_{gas}—and the second, avalanche-type growth, which is $\sim$0.15 Gyr for all models. The peak growth rate of the CMC is attained around the peak of the bar strength.

3.1. *Results: Adding the Central BH*

In models G05BH–G8BH, the bar-triggered radial gas inflow leads to the gas accumulation in the central region as well as in the fueling of the central BH surrounded by gas. Figures 2 and 3 demonstrate both the growth of the BH mass, $M_\bullet(\tau)$, and that of the CMC within the central 250 pc, $M_{CMC250}(\tau)$, which includes the BH, gas, stars, and DM, as a function of time. Subsequently to the bar decay from its maximal strength, the growths of $M_\bullet(\tau)$ and $M_{CMC250}(\tau)$ saturate within $\lesssim$0.2 Gyr, i.e., almost instantly. The subsequent evolution of the CMC and the BH is very mild. The final $M_\bullet$ and M_{CMC250} scale linearly with the initial gas fraction in the disk. A fraction $\sim$65%–75% of the gas ends up in the CMC in all models with the BH; for smaller f_{gas} there is fractionally more gas in the end (Fig. 3). Overall, we do not find a substantial difference between the CMCs in models with and without the central BH. However, models with larger f_{gas} grow more massive BHs and CMCs affecting the subsequent bar evolution, both its vertical and planar structures, as we discuss in § 5.

4. TESTING THE MODELS

Models with an increasing gas fraction, both with and without the BH, exhibit continuity of bar properties. All of them develop bars of nearly identical strength when measured by the A_2 amplitude. Even more spectacular is the subsequent decrease in the bar strength shown in Figure 1. While the shape of $A_2(\tau)$ differs among the models, the amount of the postmaximum drop is the same. Because the models differ in the gas fraction f_{gas}, the evolution of the CMC and of the central BH will differ as well. Comparison of Figures 1–3 shows that the presence of the SBH has only a minimal influence on the bar strength, its pattern speed, and the CMC. We therefore consider the models with the BH as representative and base our discussion on them. Difference between the models is mentioned only when it is substantial.

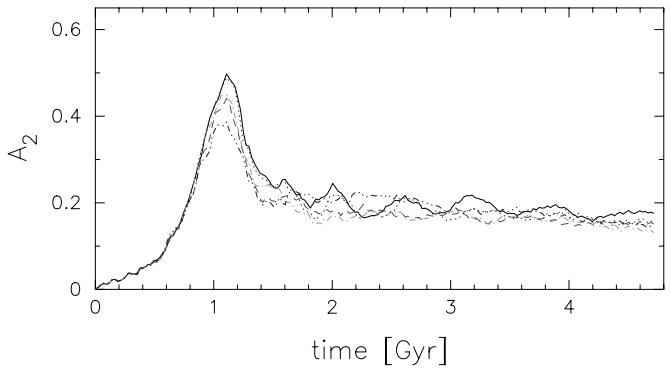

FIG. 4.—Evolution of G8 model with gradually subtracted torques from the gas onto the stars. Shown are models with 25% torques subtracted (*dotted line*), 50% subtracted (*dash-dotted line*), 75% subtracted (*dashed line*), and 100% subtracted (*dash–triple-dotted line*). For the comparison we also display G8 (*solid line*). [*See the electronic edition of the Journal for a color version of this figure.*]

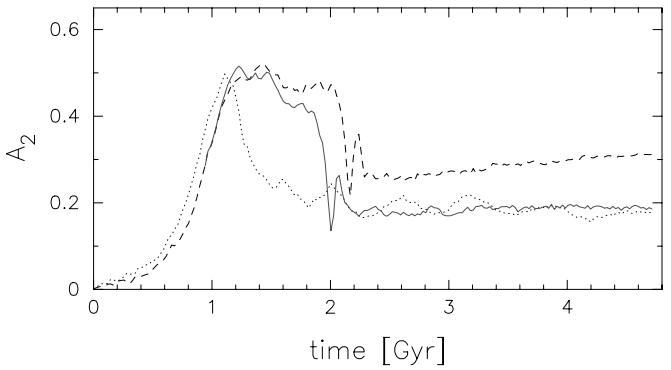

FIG. 5.— Evolution of A_2 in the G0GT model (*solid line*), constructed from the G0 model under the gravitational torques from the gas onto the stars in G8BH. For the comparison we also display G8BH (*dotted line*) and G0 (*dashed line*). [*See the electronic edition of the Journal for a color version of this figure.*]

4.1. *Removing Gas Gravitational Torques on Stars*

The stellar and gas fluids differ in their intrinsic physical properties, specifically in viscosity, which generates the time lag in the gas response to any perturbation. This time lag is the source of gas-stars mutual gravitational torques within the bar (eq. [1]); with no viscosity the contribution of this integral is zero. The angular momentum within the bar flows from the gas to the stars in the disk and to a certain degree to the DM halo. Removing these torques and comparing the models will allow for a direct testing of Bournaud et al. (2005) claim that they affect the stellar bar evolution.

Because we aim at understanding the effect of the gas on the bar evolution, specifically through angular momentum redistribution in the system, we use the bar strength measured by A_2 and follow the balance of the angular momentum in the basic morphological components—the disk, bar, and DM halo. We first ask the question, to what degree is the gas responsible for the bar weakening shown in the Figure 1*a* frames? We test the possibility that the large drop in the bar strength shown in the various models of Figure 1*a* between $\tau \sim 1$ and 2.5 Gyr results from the input of the angular momentum coming from the gas gravitational torques, as proposed by Bournaud et al. (2005).

The fact that G0, the pure stellar model, shows the same qualitative behavior as other models and that the degree of weakening is even quantitatively similar raises serious doubts that the gas is in any way responsible for the bar downsizing. Nevertheless, we perform the first test of removing a fixed fraction of the gravitational torques, by removing the tangential components of the gravitational forces, applied by the gas on the stars and the DM. Figure 4 exhibits four models based on G8BH in which the torques have been reduced by 25%, 50%, 75%, and 100%, i.e., models G8-25T–100T. It shows that there is no substantial difference between the G8BH and G8-T models. While the A_2 peak around 1.1 Gyr lowers slightly, when the torques are removed, we consider this to be a numerical rather than physical effect. For example, differences of this level are even expected for the same model that uses a different random "seed" in the initial conditions. The subsequent evolution of models in Figure 4 shows a clear convergence trend. While indeed the stellar bar receives less angular momentum from the gas, one is forced to conclude that the gas torques have no effect on the observed drop in the bar strength in our models. The question of course is, what is the origin of this drop? We address this issue in § 5 after exploring various venues via test models.

4.2. *Gas Substitutes*

In tandem with tests shown in Figure 4, we advanced the G0 model with artificially added gravitational torques from the gas in G8BH model. For this purpose, we calculate the torques from the gaseous component on a Cartesian grid for the (total) dimension of 50 kpc × 50 kpc × 4 kpc. The (constant) grid spacing is 250 pc along the *x*- and *y*-axes and 2 kpc along *z*. In order to have a smooth force field, we take time average over several frames. We bring up the force field quasi-adiabatically between $\tau \sim 0.94$ and 1.22 Gyr (Fig. 5), or over 20 dynamical times, reaching its full strength about the time when the bar amplitude also reaches its maximum. To apply the torques on the stellar and DM components, we use a 2D spline interpolation.

The resulting evolution (model G0GT) follows closely that of the G8BH model, with the exception of the A_2 drop time, i.e., the extent of the associated plateau. Both tests performed in this section agree with our previous conclusion that for models with $f_{\rm gas} \lesssim 8\%$, the gravitational torques from the gas do not alter substantially the drop in the A_2 observed in all models, but have a profound effect on the extent of the plateau that precedes the drop. They also serve as an independent verification that our modeling of effects of the gas component is sufficiently reasonable and does not alter the model evolution in some unexpected way.

4.3. *Artificial Growth of the BH and the CMC*

The stellar bar is expected to evolve with respect to the buildup of the central BH and the nearby gas accumulation. If these grow on a secular timescale, i.e., adiabatically, this gas will drag in additional stars and DM. The evolution of the mass within the central 250 pc and the central SBH are shown in Figures 2 and 3 for models with various $f_{\rm gas}$.

To further isolate the consequences of a gas influx toward the central regions, we have used the pure stellar model G0 and imposed the BH and gas accumulation histories taken from a gas-rich model. The CMC is defined as earlier and consists of the gas accumulation within the central 250 pc (or 750 pc) and the stars and DM there. Figure 6 shows two such models: an artificially growing BH taken from the G8BH (model G0BH), and an additional model of a growing BH from G8BH when the gas within the central 250 pc is added to the BH mass model (G0BH250). In both cases the gravitational softening of the BH is 160 pc—the typical softening in our models. The model G0BH closely follows

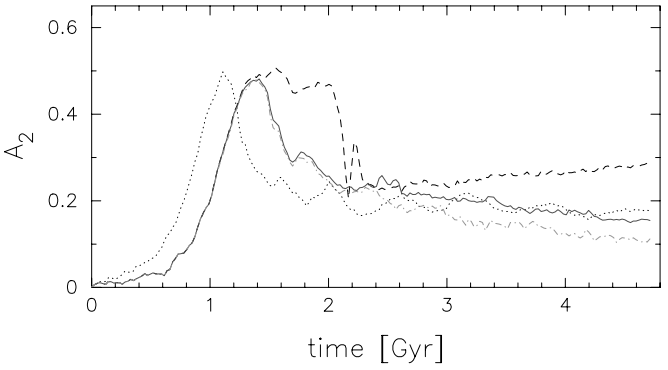

FIG. 6.—Evolution of A_2 in the G0BH model with an artificially grown BH, whose history is taken from G8BH (*solid line*), and the G0BH250 model with an artificially grown BH and the gas within the central 250 pc (added to the BH mass) (*dash-dotted line*). G0 (*dashed line*) and G8BH (*dotted line*) curves were added for a comparison. [*See the electronic edition of the Journal for a color version of this figure.*]

the corresponding G8BH, although no gravitational torques from the gas are present here. The A_2 curve has switched gradually from that of G0 to G8BH. The corresponding model G0BH250 with more massive SBH (as the gas within the central 250 pc has been added to the BH) falls below the G0BH curve, as expected; this confirms that more massive SBHs, albeit not found in disk galaxies by a large margin, can in fact dissolve the stellar bars, as discussed in the literature.

Figure 7 displays, first, the evolution a BH with an added gas mass from the central 250 pc but with the gravitational softening of the BH decreased to 80 pc (model G0BH80), to test a more compact mass distribution, and second, a growing BH and an independently growing gas accumulation within the central 750 pc (model G0BH750). This gas is approximated by a second Plummer sphere with a characteristic radius of 750 pc. The G0BH80 bar decays gradually and its A_2 fall below that of G0BH250; smaller gravitational softening for the BH creates a more compact CMC here that starts to affect the bar secularly. The substantially more massive CMC in G0BH750 has a profound effect on the bar by dissolving it during $\sim$5 Gyr, as discussed in § 1.

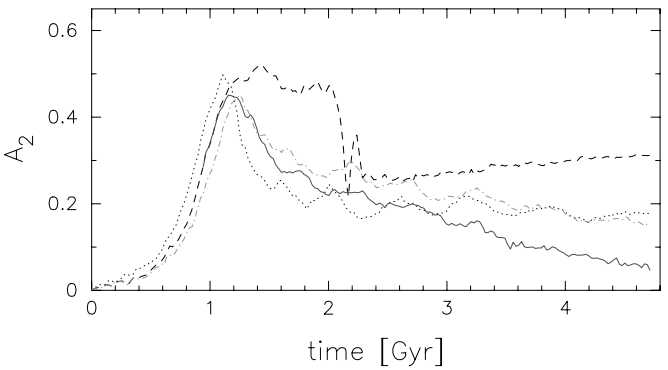

FIG. 7.—Evolution of A_2 in the G0BH80 model with an artificially grown BH with a smaller gravitational softening of 80 pc, whose history is taken from G8BH and is a combined mass of the SBH and the gas within the central 250 pc (*solid line*), and the G0BH750 model with an artificially grown BH (regular softening of 160 pc) and the gas within the central $r_0 = 750$ pc, which is modeled as a Plummer sphere with r_0 (*dash-dotted line*). G0 (*dashed line*) and G8BH (*dotted line*) curves were added for a comparison. [*See the electronic edition of the Journal for a color version of this figure.*]

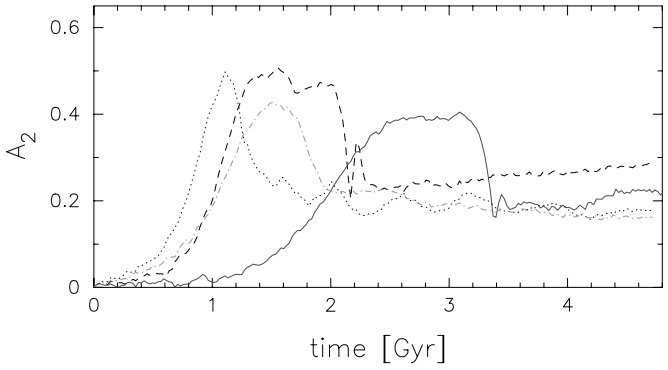

FIG. 8.—Evolution of A_2 in G0-Q18 (*solid line*) and G8BH-Q18 (*dash-dotted line*) models, which are similar to G0 and G8BH but with $Q = 1.8$. For the comparison we also display G8BH (*dotted line*) and G0 (*dashed line*). [*See the electronic edition of the Journal for a color version of this figure.*]

4.4. *Stellar Bars in Hot Disks*

Stellar bar instability is delayed and its amplitude is lowered in hotter disks, i.e., disks with larger stellar dispersion velocities (e.g., Athanassoula & Sellwood 1983). In order to test this effect on the abrupt weakening of the bar in our models, we have increased the initial Q parameter to 1.8 in the G0 and G8BH models, hereafter models G0-Q18 and G8BH-Q18. Figure 8 displays the evolution of these models. The rise time of the bar instability has increased as expected in both models, and the A_2 peaks are delayed with respect to the original models. The maxima of the A_2 amplitudes have been also lowered by $\sim$0.1, and the amplitude of the drop in A_2 has diminished by this amount as well. The difference between the above models after the amplitude drop decreases substantially. The stellar bars survive and do not show any sign of decay over the simulation time of 5 Gyr.

4.5. *Angular Momentum Evolution*

Next, we analyze the angular momentum (J) redistribution between the disk and the DM halo in the presence of the gas. The resonant interaction between the various morphological components will be addressed elsewhere. We have divided the disk/halo system into the (cylindrical) part within the CR and outside it. The overall J of the DM halo increases sharply only after the bar has reached it maximal amplitude, i.e., after $\sim$1 Gyr, and is larger by a factor of $\sim$2 for the gas-poor models than for G8. The inner and outer halos (with respect to the bar CR) follow the same trend, with the outer halo gaining more than the inner one.

The angular momentum of the disk is decreasing steadily, more sharply after $\sim$1 Gyr, in all models. This decrease is a result of the J loss by the inner disk over this time period. Subsequently, this J increases very slightly in the gas-poor models and saturates in gas-rich models. The outer disk behavior traces (anti)symmetrically that of the inner disk. The gas in the inner disk possesses a small fraction of J (i.e., in the stellar disk) even in gas-rich models evolved here and rapidly loses it during the first Gyr, then stays flat for the remaining of the simulations. So, J in the system flows from the inner disk to the outer disk and to the halo. The inner halo responds to this trend, largely because of the appearance of the "ghost" bar in the DM there (Athanassoula 2005; Berentzen & Shlosman 2006).

The role of gas in the overall balance of J in the disk/halo system can be estimated from Figure 9. Here we compare the direct input of J into the stellar disk via the gravitational torques from the gas with the total flow of J in the disk. The upper solid lines show the input of J by the gas to the stars by integrating over the

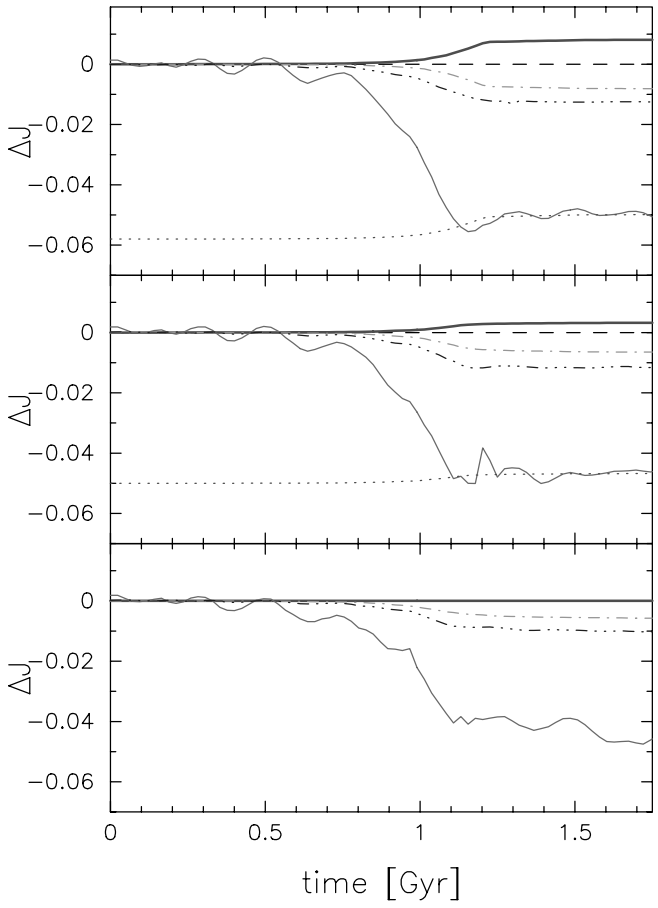

FIG. 9.—Change in the angular momentum (ΔJ) within the CR radius in G8BH (*top*), G8-50T (*middle*), and G8-100T (*bottom*). The upper solid lines show J flow from the gas to the stars calculated from integration of corresponding gravitational torques. The dash-dotted lines provide the J flow from the stars to the gas, calculated from the torques as well. The dash–triple-dotted and lower solid lines exhibit the J flow in the gaseous and stellar component, respectively, calculated directly from model evolution. The dotted lines are identical to the upper solid lines shifted to match the lower solid lines. The dashed line is added to emphasize the $\Delta J = 0$ line. [*See the electronic edition of the Journal for a color version of this figure.*]

torques in models with gradually reduced torques, G8BH, G8-50T and G8-100T. The lower solid lines describe the total ΔJ in the stellar component. The dotted line is identical to the upper solid one but shifted downward for a direct comparison with the lower solid line. The J input by the gas into the stars over 5 Gyr of the run is ~13% of the stellar J loss to the DM halo over this time. This relatively small input explains the near independence of the bar strength on the gas torques. However, as we discuss in the next section, the gas accumulation in the center resulting from the stellar bar has a profound effect on the evolution of the vertical structure in the bar.

5. DISCUSSION: BAR EVOLUTION AND GAS

The main goal of this work is to understand the effect of gas on stellar bar evolution. For this purpose we have run a series of models for stellar disks embedded in live DM halos, with various gas fractions ranging from 0% to 8% of the disk mass, with and without a growing central BH. In all of these models, the bar growth is barely affected by the gas presence; more gas-rich models display a marginally shorter rise time of the bar instability. The maximal values of the bar amplitude, $A_2 \sim 0.5$, attained by the bar are very similar in all models. Past this maximum, the gas-poor models exhibit a plateau in A_2 for about 1 Gyr, followed by a sharp drop in the amplitude to ~0.2. This plateau gradually disappears with increasing $f_{\rm gas}$, and its extent clearly anticorrelates with the CMC mass. Subsequently, the models differ in their evolution, ranging from a slight decline to a slight increase in A_2; this evolution clearly separates gas-poor (G0–G2; $f_{\rm gas} < 3\%$) from gas-rich (G4–G8; $f_{\rm gas} > 3\%$) models. In all models the stellar bar has survived during the computation time of 5 Gyr, although appears to be substantially weakened. Models with growing BHs show no significant difference in their evolution compared to models without the BH.

Additional models testing the importance of various parameters for the dynamical and secular evolution of bars have been advanced. First, ~25%–100% of the gravitational torques that the gas exerts on stars have been removed in our most gas-rich model with $f_{\rm gas} = 8\%$. This barely affected the A_2 curve. Second, we have added the gas "force field" from our gas-rich model to the purely stellar model; the A_2 curve switched its behavior and closely followed the original gas model, preserving the same drop in A_2. Third, we have run a number of pure stellar models, which have grown the SBHs and the CMCs artificially, using their histories from the gas-rich model. No gravitational torques from the gas onto the stars have been present, but the bar strength has shown the same sharp decay. Fourth, pure stellar and gas-rich models have been run in hotter disks with initial $Q = 1.8$; these have shown qualitatively similar behavior, with bars reaching lower amplitudes but exhibiting the same drop in A_2. Finally, the amount of gas J transferred to the stellar bar is small compared to the overall J balance there.

The conclusion that emerges from these runs is that a *direct* input of the angular momentum from the gas into the stellar bar is not responsible for the sharp drop in its strength, even in the gas-rich models. It is most revealing that the pure stellar model shows no qualitatively different behavior from models with various gas fractions. Only with an additional analysis of the bar structure do the differences in evolution between the gas-pure and gas-rich models start to emerge, as we discuss below.

5.1. *Pure Stellar Models: Drop in the Bar Strength*

We now attempt to address the issue of what is the origin of the sharp weakening of the bar in G05–G8 and G05BH–G8BH models with gas. The pure stellar model G0 acts here as the Rosetta Stone: the reason for the drop in its amplitude, A_2, is the increasing fraction of chaotic orbits within the bar (Martinez-Valpuesta & Shlosman 2004). This behavior is triggered by the dynamical (buckling) instability, first detected in Combes & Sanders (1981) and analyzed by Combes et al. (1990), Pfenniger & Friedli (1991), Raha et al. (1991), and others, largely based on Toomre (1966) interpretation. The buckling instability is characterized by a spontaneous break of the symmetry with respect to the disk equatorial plane. It results in the vertical thickening of the bar that acquires a characteristic boxy/peanut shape, frequently observed in edge-on disks along the bar minor axis (e.g., Lütticke et al. 2000).

However, formation of the characteristic boxy/peanut shape of the inner bar does not necessitate the buckling instability. Friedli & Pfenniger (1990) have shown that the near suppression of the vertical asymmetry in the bar still results in this characteristic shape, albeit established on a much longer *secular* timescale. They found that the bar thickening can be a direct consequence of the heating in the bar by its vertical inner Lindblad resonance (ILR) and other lower resonances that scatter the stellar particles out of the disk plane.

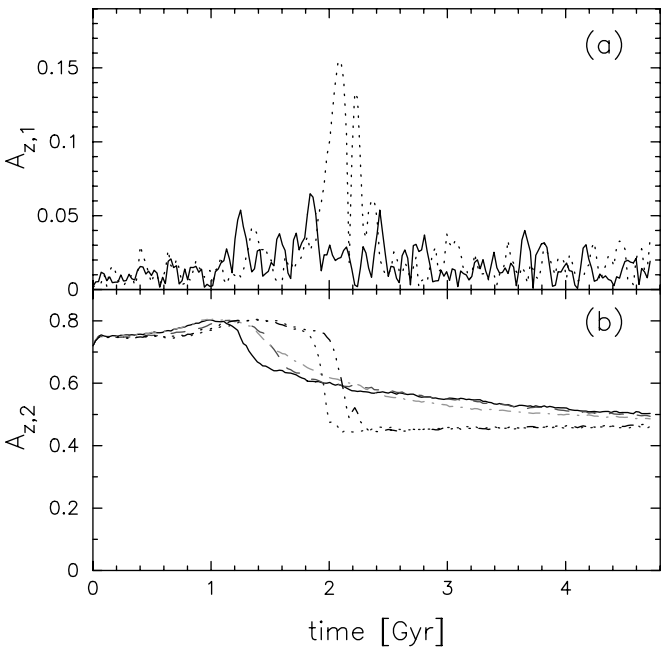

FIG. 10.—(*a*) Vertical asymmetry of the disk measured by $A_{z,1}$ Fourier coefficient. Shown are G0 (*dotted line*) to G8BH (*solid line*) models. (*b*) The vertical "strength" of the stellar bar measured by $A_{z,2}$ for G8BH (*solid line*), G6BH (*dashed line*), G4BH (*dash-dotted line*), G2BH (*dotted line*), and G0 (*dash–triple-dotted line*) models. [*See the electronic edition of the Journal for a color version of this figure.*]

These two alternatives for the bar to obtain the characteristic peanut shape can be reconciled. The initial growth of the stellar bar is accompanied by a strong increase in the chaotic motions in the *x*-*y* plane, especially in its outer part beyond the vertical ILR and close to CR. These motions are the prime reason for the outer bar dissolution and its *overall* weakening in the *x*-*y* plane; the bar actually shortens dramatically over a fraction of a Gyr. What is most important is that *the role of the buckling is to accelerate the otherwise secular* (*vertical*) *heating to a dynamical timescale* (Martinez-Valpuesta & Shlosman 2004). Particles that are normally confined to the bar equatorial plane are injected above it, allowing them to explore a larger configuration space. Hence one can distinguish between the buckling that is a dynamical instability and the action of the resonances that drive a slow vertical diffusion of the planar stellar orbits.

The model G0 exhibits just such a behavior that weakens the bar in the *x*-*y* plane but does not lead to a complete bar dissolution. It displays a strong vertical asymmetry at $\tau \sim 2$–2.3 Gyr as given by the (vertical) Fourier coefficient $A_{z,1}$, which has a maximum at this time (Fig. 10*a*), and the vertical bloating given by another Fourier coefficient in the vertical plane, $A_{z,2}$ (Fig. 10*b*). The initial growth of the stellar bar triggers two processes that appear to be nearly fatal for the bar itself. First, a larger fraction of stellar orbits in the bar become chaotic. The readily developing vertical ILR is located within the bar (typically half-way to the CR radius) and efficiently scatters (randomizes) the orbits in the bar vertical plane. Particles whose energy allows them to visit the outer part of the bar inevitably will cross the resonance region and will be affected most, thus dissolving the outer half of the bar. It is possible, but remains to be proven, that the first particles scattered above the disk plane act as "seeds" for the (collective) buckling instability. This would explain why the appearance of the vertical ILR and the onset of the dynamic instability happen so close in time.

Strengthening of a stellar bar increases the importance of the vertical ILR and other lower resonances; this widens the associate resonance gaps in the characteristic diagrams.[4] The ILR gap gives rise to specific symmetric/antisymmetric orbital families, called BAN/ABAN[5] correspondingly (Pfenniger & Friedli 1991; Berentzen et al. 1998; Skokos et al. 2002; Martinez-Valpuesta et al. 2006). These orbits are the 3D counterparts of the planar x_1 orbits introduced by Contopoulos & Papayannopoulos (1980) and become populated when the planar orbits are destabilized. The BAN/ABAN orbits imprint their characteristic boxy/peanut shapes on the (inner) bar, in tandem with other 3D families that originate at lower resonances. When the vertical symmetry in the bar is enforced, the population growth on these orbits is a slow secular process developing over many rotations of the bar.

5.2. *Gas Models: Drop in the Bar Strength and Quenching the Bar Buckling*

All models with the gas, shown in §§ 3 and 4, exhibit a drop in A_2 that is similar to the drop in the pure stellar model. Because the initial conditions for all these models are the same, and the evolution toward the peak in A_2 and the subsequent drop are nearly identical, it is tempting to assume that the same population of stellar orbits leaves the bar either as a result of the buckling or the action of the CMC. This population has been identified by Martinez-Valpuesta & Shlosman (2004) as consisting mainly of chaotic orbits developing in the bar midplane. We do not pursue this line further here. The orbital nomenclatures are discussed in Berentzen et al. (1998) and in Patsis et al. (2002).

Evolution of the bar vertical shape is further complicated by the presence of the gas component. The amplitude of the vertical buckling, as measured by $A_{z,1}$, shows a twofold behavior: gas-poor models exhibit a substantial buckling, while gas-rich models remain nearly symmetric (Fig. 10*a*). Berentzen et al. (1998) found that in the presence of gas, the vertical instability in the bar is damped substantially. The new detail that emerges here is that *while the bar remains symmetric in the gas-rich models, it nevertheless thickens*. In the gas-poor models, the bars thicken abruptly and subsequently remain unchanged, in the sense that the vertical swelling saturates immediately thereafter. In the gas-rich models, one can clearly distinguish two phases—an initial and fast swelling and a subsequent increase in the vertical thickness. This bimodal behavior is clearly displayed in Figures 10*b* and 11. The former figure contrasts the vertical $A_{z,2}$ coefficient in G0 and gas models; the bulge forms nevertheless, but its boxy/peanut shape becomes progressively less prominent (as observed and quantified first by Berentzen et al. 1998, and confirmed by Athanassoula et al. 2005). Figure 11 supports this conclusion through the measure of a new parameter $\gamma \equiv (1/N_0)\sum_i z_i/r_i$ and its counterpart $\tilde{\gamma} \equiv (1/N_0)\sum_i |z_i/r_i|$ for the stellar particles in the more gas-rich models, with and without the BHs. Here we sum over the cylindrical region of 0 kpc $\leq r \leq 10$ kpc and $|z| \leq 1$ kpc, and N_0 is the number of stellar particles within this region used here for a normalization. These parameters quantify the (vertically) asymmetric and symmetric particle distributions, respectively. They appear less noisy than $A_{z,1}$.

The trend in $A_{z,1}$, $A_{z,2}$, γ, and $\tilde{\gamma}$ that separates the gas-rich from the gas-poor models can be explained by the presence of the CMC. The growth of the CMC in our models is clearly linked to

[4] These diagrams plot the *y*-intersection of a stellar orbit against the associated integral of motion, the Jacobi energy E_J (e.g., Binney & Tremaine 1987).

[5] These are 2:2:1 orbits, i.e., two radial oscillations for two vertical oscillations for one azimuthal turn.

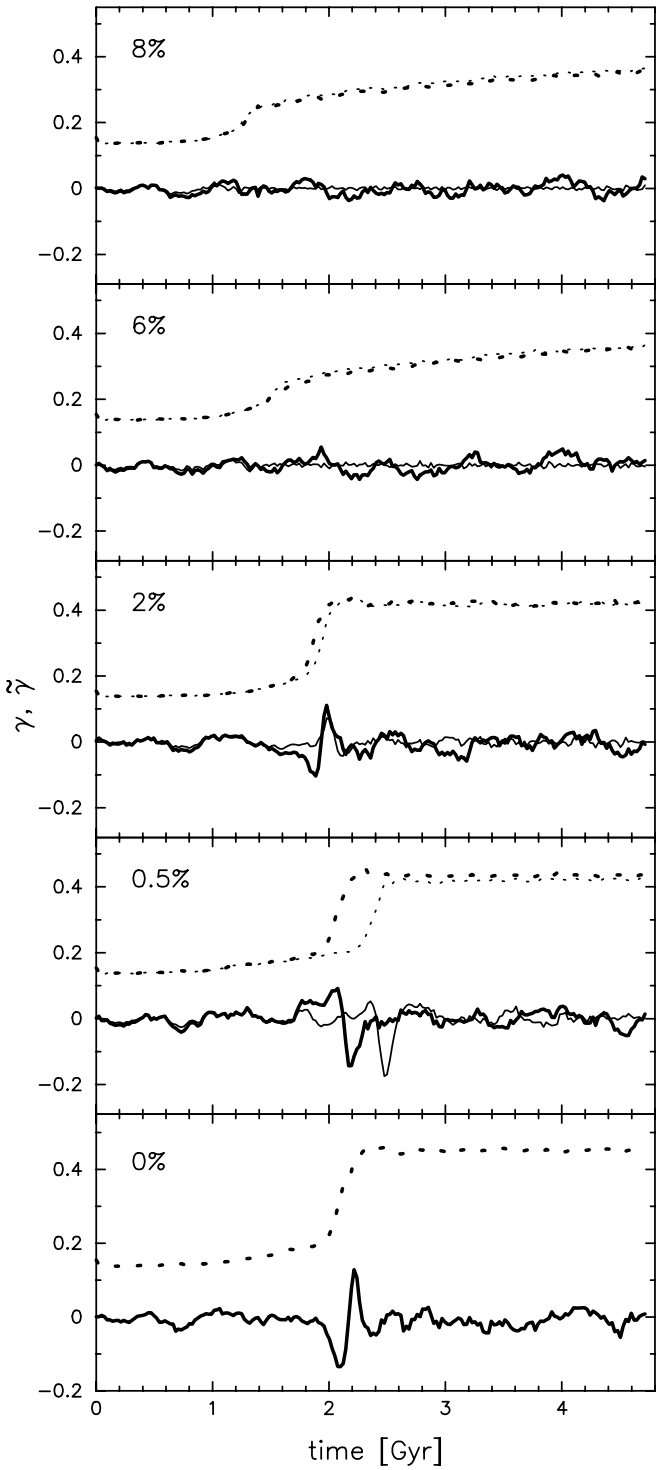

FIG. 11.—Vertical thickening of the bar $\gamma \equiv (1/N_0)\Sigma_i z_i/r_i$ (*solid lines*) and $\tilde{\gamma} \equiv (1/N_0)\Sigma|z_i/r_i|$ (*dashed lines*) in models with $f_{\rm gas}$ of 8%–0% (*top to bottom*). Thin and thick lines correspond to models with and without the SBH.

the gas, as the purely stellar model forms virtually no CMC.[6] On the other hand, the final mass of the CMC depends linearly on $f_{\rm gas}$ in our models. Such massive CMCs will have immediate implications on the formation and shapes of galactic bulges and on the onset of the bar buckling. They destabilize the BAN/ABAN orbits,

[6] The only contribution to the CMC in the stellar models comes from the stellar and DM ghost bars.

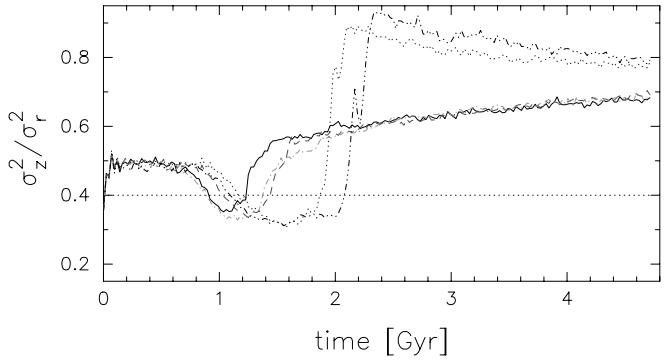

FIG. 12.—Evolution of $\beta \equiv \sigma_z^2/\sigma_r^2$, the ratio of vertical dispersion velocities in G8BH (*solid line*), G6BH (*dashed line*), G4BH (*dash-dotted line*), G2BH (*dotted line*), and G0 (*dash–triple-dotted line*) models. β is calculated using dispersion velocities within the central kpc. The dotted line at $\beta = 0.4$ corresponds to the buckling instability limit for a wide range of models here and elsewhere. [*See the electronic edition of the Journal for a color version of this figure.*]

whose stable regions shrink toward the disk midplane; this damps the vertical asymmetry, reducing support for the boxy/peanut bulge shapes (Berentzen et al. 1998; Athanassoula et al. 2005). The increase in the stellar velocity dispersions proceeds both on dynamical and secular timescales, and is driven by resonant and nonresonant mechanisms, as we discuss below.

The action of the vertical resonances follows from the spatial part of the stellar distribution function, while its kinematic part drives the stellar vertical-to-radial velocity dispersion ratio, $\beta \equiv \sigma_z^2/\sigma_r^2$. The latter behavior is displayed in Figure 12. We find that σ_r initially increases with time, which is related to the bar strengthening. At $\tau \sim 2$–2.3 Gyr, for G0 and the gas-poor models, β increases sharply from $\sim$0.3 to $\sim$0.9. This jump brings β to nearly isotropic conditions, and its mere appearance signifies a sudden change in the vertical structure of the bar—stellar settling on the BAN/ABAN orbits. The subsequent gradual decrease in β follows from a secular increase in σ_r and is related to the slow growth of the bar.

While an exact value of β, when the buckling instability is triggered, can depend on a particular model, within limits, we find that it lies around $\beta \sim 0.4$ for models presented here and in Martinez-Valpuesta et al. (2006). This value agrees well with that of Sellwood (1996), who found that some of his models remained unstable for up to $\beta \sim 0.4$.

The gas-rich models behave systematically different from the gas-poor models in Figure 12, as much as they differ in Figures 10 and 11. While β still drops below the threshold of 0.4, as the buckling develops, a steep growth of the CMCs in these models produces an equally abrupt heating of the stellar "fluid"—an increase in the stellar dispersion velocities within the central kpc. This drives β above the threshold and suppresses the buckling instability—a nonresonant effect. The comparative increase in σ_r prevents β from growing to values attained in the gas-poor models. It is of a prime importance that the vertical heating of σ_z is independent of $f_{\rm gas}$, in tandem with the similar behavior of A_2 in all models. The subsequent secular increase in β is driven by an increase in σ_z and is related to the action of the vertical resonances discussed earlier.

In a number of control runs (e.g., § 4), we have added the CMCs of various mass and compactness to the pure stellar model. The resulting $A_{z,1}$ and $A_{z,2}$ evolution remained twofold and followed either the gas-poor or gas-rich models, although no gravitational torques from the gas onto the stars were involved. Models G0BH and G8BH250 behave as gas-poor, while G0BH80 and

G0BH750 as gas-rich, displaying substantial or negligible vertical asymmetries correspondingly, but the overall thickening of the bar at the end of the simulations is similar to that in the pure stellar model.

5.3. *The Bulge Shape: Effect of the Gas*

The gradual loss of the characteristic shape of the bulge is correlated with increasing $f_{\rm gas}$ in our models. The peanut shape is replaced by the boxy one and by an increasingly elliptical bulge (especially in the inner isodensities). In the gas-poor models, the increase in the velocity dispersion discussed earlier injects stellar particles above the disk. During the buckling instability, a spontaneous breakup of the vertical symmetry occurs: σ_z increases and σ_r decreases (because the hottest particles in the x-y plane leave it). The vertical velocity dispersion (i.e., degree of freedom), σ_z, in the disk is an adiabatic invariant and is affected by this dynamical instability.

For the gas-rich models, the steep increase in the CMC mass (see Figs. 2 and 3) pumps energy in both the vertical and horizontal planes: σ_z and σ_r increase simultaneously. This heating of the stellar disk in the x-y and vertical planes is the result of a strong *planar* ILR that develops in the gas-rich models, in addition to the vertical ILR that is present even in the gas-poor models. This was explicitly shown by Berentzen et al. (1998) for both types of models using identical initial conditions to those presented here. As a result, the Jacobi energy of stellar particles—normally a conserved quantity, increases abruptly, and particles are injected on 3D orbits above the disk that are not trapped by the BAN/ABAN family. These orbits reduce support for the boxy/peanut shape of the bulge, which becomes progressively rounder with $f_{\rm gas}$, as observed in our simulations.

An additional effect can contribute further to the damping of the vertical asymmetry in the gas-rich models. The condition for a linear vertical buckling of thin sheets with radial dispersion velocities has been analyzed by Toomre (1966). For pure collisionless systems, the instability saturates in the nonlinear regime because of wave-particle and wave-wave damping (e.g., Sellwood et al. 1998). In the presence of a substantial gas component, a strong damping originates in the two-fluid gas-stars interaction. The source of this damping is in the overall response mismatch between the collisionless disk and the viscous gas. The difference in the stellar and gaseous responses can be noticed already in the linear regime, by applying the epicyclic approximation. Using Heller & Shlosman (1996) notation, we follow the vertical oscillations at some radius r, regardless of the excitation cause. While the stellar component follows the harmonic oscillator equation $\ddot{Z}_1(\tau) + \nu^2 Z_1(\tau) = 0$, the gas follows the damped oscillator equation, $\ddot{Z}_1(\tau) + \lambda \dot{Z}_1(\tau) + \nu^2 Z_1(\tau) = 0$, where the subscript "1" represents the first-order terms, ν is the vertical epicyclic frequency, λ (>0) is the damping coefficient in the gas, and the dots denote the time derivatives. The formal solution to the second equation is $Z_1(\tau) = A(\tau, \lambda) \cos(\omega\tau + \delta)$, where $A(\tau, \lambda)$ is the time-dependent (decaying) amplitude of the oscillation, $\omega = \omega(\nu, \lambda)$, and δ provides the phase-shift between the gaseous and stellar responses. This phase-shift depends explicitly on the λ and disappears when $\lambda \rightarrow 0$.

The vertical oscillations that accompany the buckling instability are clearly visible in the numerical simulations of a pure stellar disk embedded in a live DM halo of Martinez-Valpuesta et al. (2006, see their accompanying animation), and we observe them here as well. The gas component buckles as well but immediately falls back to the disk midplane and remains unperturbed thereafter. The reason for this difference in behavior is the dissipation present in the gas: this prevents the BAN/ABAN orbits, which have sharp turns, from sustaining the gas.

Hence, the action of the CMC is to suppress the vertical buckling in stellar bars with larger gas fractions, above a few percent of the disk mass, and to increase the stellar dispersion velocities. This weakens the boxy/peanut shape of the bulge and shortens the plateau in A_2. In the long run, the inner bar thickens additionally due to the secular action of the vertical resonances. So the development of the boxy/peanut bulges appears to be limited by the gas influx to the center in the gas-rich disks. This has been noted by Berentzen et al. (1998) using a lower resolution model, and by Athanassoula et al. (2005) using an analytical potential for the CMC. In the latter work, the CMC has been introduced after the boxy/peanut-shaped bulge has formed, while here we find that the growth of the CMC can weaken the orbital support for this shape in the first place. Of course, the star formation will be important in altering the gas accumulation in the center and will affect the bulge morphology in some way. Future numerical modeling will quantify this process.

This means that the galactic stellar bars go through vigorous evolution not only in the equatorial disk plane but also in the plane normal to the disk. Geometrically thin bars in *both* planes readily develop a large population of chaotic orbits that "leak" and thicken the bar over (at least) secular but sometime dynamical timescales. The gas inflow toward the central few hundred parsecs, while damping the vertical buckling, heats up the stellar disk; this is a vigorous heating that proceeds on dynamical and secular timescales. We find that β still drops below 0.4 (Fig. 12) and that the vertical heating is not driven by the spiral structure in the disk, as claimed by Debattista et al. (2006); the heating exists even in a pure stellar model with a massive CMC that has no spiral structure. Furthermore, while the gas of course participates in the buckling itself, the gas layer remains thin and quickly collapses to the disk midplane; this result is not related to the isothermal EOS and persists for adiabatic gas as well. The only residual swelling of the gas layer comes from its response to the background stellar potential, which becomes shallower with time.

The effect of the CMCs on the evolution of stellar bars in our simulations is important in determining the bar vertical and planar structure over the simulation time. Although we have limited the length of the evolution to $\sim$5 Gyr, this is a substantial period of time to assess the immediate influence of the CMCs. Beyond shortening the plateau around the maximum in A_2, the main difference between gas-poor and gas-rich models lies in that former show bars that resume their growth after the period of buckling instability. The latter models display bars that exhibit a mild weakening.

The SBH masses in our simulations attain $\sim$0.3%–5% of the disk mass, depending on $f_{\rm gas}$. From the observational point of view, this appears to be a factor of $\sim$10 in excess of the SBH masses observed in disk galaxies. What is interesting is that even these large masses do not lead to a dissolution of stellar bars even over the time periods of 5 Gyr. This result is in sharp contrast with the modeled bars of Friedli (1994), which decay completely over 1–2 Gyr, but in agreement with Athanassoula et al. (2005), who report much more robust bars. One possible explanation lies in the absence of a DM halo in the former simulations. Under these conditions, the stellar bars develop faster, become stronger, and have a larger fraction of chaotic orbits. The dissolving action of the SBH will be much more formidable in this case.

5.4. *Summary*

In summary, galactic bars in our simulations go through various stages of evolution, and we focus primarily on changes in the bar mid- and vertical planes. The pure stellar bars have been analyzed in this context in the literature (e.g., § 1); our goal was to understand how the gas presence modifies this evolution, in the

range of $f_{\rm gas} \lesssim 8\%$. A large number of models of a two-component disk embedded in the live DM halo have been analyzed. We find a twofold evolution and contrast the gas-poor, $f_{\rm gas} < 3\%$ with the gas-rich, $f_{\rm gas} > 3\%$ models. The exact dividing line, $f_{\rm gas}$, between these groups can vary, but the essence remains.

First, the angular momentum transfer from the gas to the stellar bar has no visible effect on the evolution of the bar strength in our models, beyond a well-known buildup of the CMC and the SBH there, contrary to Bournaud et al. (2005). We find that more massive CMCs shorten dramatically the extent of the plateau near the maxima of the bar strength. Second, all stellar bars thicken vertically, but the reason is twofold: gas-poor models buckle while gas-rich models swell by preserving their symmetry. The vertical asymmetry (buckling) of the bar is damped in gas-rich models due to the forming CMC. Third, the vertical swelling starts earlier for the gas-rich disks and this effect increases with $f_{\rm gas}$. Fourth, the vertical thickening of a stellar bar proceeds in two stages. Namely, the CMC heats up the central kpc in the stellar disk on a dynamical timescale; this stabilizes the bar against buckling, but puffs it up. This is followed by a *slow* (secular) stage of the bar thickening that complements the dynamical stage. Overall, the degree of the stellar bar thickening is practically *independent* of the gas fraction in the disk, for $f_{\rm gas} \lesssim 8\%$. Fifth, the action of the CMC leads to the formation of a weaker peanut and more elliptical bulge, in a contrast to the boxy/peanut-shaped bulge forming in the gas-poor models, confirming the earlier result of Berentzen et al. (1998). The severity of this effect depends on the star formation process and the feedback from stellar evolution.

We acknowledge helpful conversations with Francoise Combes and Daniel Pfenniger. We thank Barbara Pichardo for helping with the initial stages of this project. This research has been partially supported by NASA/LTSA 5-13063, NASA/ATP NAG5-10823, HST/AR-10284 (to I. S.), and NSF/AST 02-06251 (to C. H. and I. S.). I. B. acknowledges financial support by the project GRACE I/80 041 of the Volkswagen Foundation. I. M.-V. is grateful for support by the Gruber Foundation.

REFERENCES

Athanassoula, E. 1992, MNRAS, 259, 345
———. 2003, MNRAS, 341, 1179
———. 2005, Ann. NY Acad. Sci., 1045, 168
Athanassoula, E., Lambert, J. C., & Dehnen, W. 2005, MNRAS, 363, 496
Athanassoula, E., & Misiriotis, A. 2002, MNRAS, 330, 35
Athanassoula, E., & Sellwood, J. A. 1983, in IAU Symp. 100, Internal Kinematics and Dynamics of Galaxies, ed. E. Athanassoula (Dordrecht: Reidel), 203
Barnes, J., & Hut, P. 1986, Nature, 324, 446
Begelman, M. C., Volonteri, M., & Rees, M. J. 2006, MNRAS, 370, 289
Berentzen, I., Athanassoula, E., Heller, C. H., & Fricke, K. J. 2004, MNRAS, 347, 220
Berentzen, I., Heller, C. H., Shlosman, I., & Fricke, K. 1998, MNRAS, 300, 49
Berentzen, I., & Shlosman, I. 2006, ApJ, 648, 807
Binney, J., & Tremaine, S. 1987, Galactic Dynamics (Princeton: Princeton Univ. Press)
Bournaud, F., Combes, F., & Sememlin, B. 2005, MNRAS, 364, L18
Buta, R., & Combes, F. 1996, Fundam. Cosmic Phys., 17, 95
Combes, F., Debbasch, F., Friedli, D., & Pfenniger, D. 1990, A&A, 233, 82
Combes, F., & Sanders, R. H. 1981, A&A, 96, 164
Contopoulos, G., & Papayannopoulos, T. 1980, A&A, 92, 33
Debattista, V. C., Mayer, L., Carollo, C. M., Moore, B., Wadsley, J., & Quinn, T. 2006, ApJ, 645, 209
Dehnen, W. 2002, J. Comput. Phys., 179, 27
Englmaier, P., & Shlosman, I. 2004, ApJ, 617, L115
Fall, S. M., & Efstathiou, G. 1980, MNRAS, 193, 189
Ferrarese, L., & Ford, H. 2005, Space Sci. Rev., 116, 523
Forbes, D. A., Norris, R. P., Williger, G. M., & Smith, R. C. 1994, AJ, 107, 984
Friedli, D. 1994, in Mass-Transfer Induced Activity in Galaxies, ed. I. Shlosman (Cambridge: Cambridge Univ. Press), 268
Friedli, D., & Pfenniger, D. 1990, in ESO/CTIO Workshop on Bulges of Galaxies, ed. B. Jarvis & D. M. Terndrup (Garching: ESO), 265
Hasan, H., & Norman, C. A. 1990, ApJ, 361, 69
Heller, C. H., & Shlosman, I. 1994, ApJ, 424, 84
———. 1996, ApJ, 471, 143
Heller, C. H., Shlosman, I., & Athanassoula, E. 2007, ApJ, 657, L65
Heller, C. H., Shlosman, I., & Englmaier, P. 2001, ApJ, 553, 661
Ishizuki, S., Kawabe, R., Ishiguro, M., Okumura, K. S., Kasuga, T., Chikada, Y., & Takashi, K. 1990, Nature, 344, 224
Jogee, S. 2006, Physics of Active Galactic Nuclei at all Scales, ed. D. Alloin, R. Johnson, & P. Lira (Berlin: Springer), 143
Jogee, S., Shlosman, I., Laine, S., Englmaier, P., Knapen, J. H., Scoville, N. Z., & Wilson, C. D. 2002, ApJ, 575, 156
Kenney, J. D. P., Wison, C. D., Scoville, N. Z., Devereux, N. A., & Young, J. S. 1992, ApJ, 395, L79
Knapen, J. H. 2005, A&A, 429, 141
Knapen, J. H., Beckman, J. E., Heller, C. H., Shlosman, I., & de Jong, R. S. 1995, ApJ, 454, 623
Kormendy, J., & Kennicutt, R. C. 2004, ARA&A, 42, 603
Lütticke, R., Dettmar, R.-J., & Pohlen, M. 2000, A&AS, 145, 405
Lynden-Bell, D., & Kalnajs, A. J. 1972, MNRAS, 157, 1
Maiolino, R., Alonso-Herrero, A., Anders, S., Quillen, A., Rieke, M. J., Rieke, G. H., & Tacconi-Garman, L. E. 2000, ApJ, 531, 219
Martinez-Valpuesta, I., & Shlosman, I. 2004, ApJ, 613, L29
Martinez-Valpuesta, I., Shlosman, I. Heller, C. H. 2006, ApJ, 637, 214
Norman, C. A., Sellwood, J. A., & Hasan, H. 1996, ApJ, 462, 114
Ostriker, J. P., & Peebles, P. J. E. 1973, ApJ, 186, 467
Patsis, P. A., Skokos, Ch., & Athanassoula, E. 2002, MNRAS, 337, 578
Pfenniger, D., & Friedli, D. 1991, A&A, 252, 75
Raha, N., Sellwood, J., James, R. A., & Kahn, F. D. 1991, Nature, 352, 411
Sellwood, J. A. 1996, in Barred Galaxies, ed. R. Buta, D. A. Crocker, & B. G. Elmegreen (San Francisco: ASP), 259
———. 2006, ApJ, 637, 567
Sellwood, J. A., Nelson, R. W., & Tremaine, S. 1998, ApJ, 506, 590
Shen, J., & Sellwood, J. A. 2004, ApJ, 604, 614
Shlosman, I. 2005, in AIP Conf. Proc. 783, The Evolution of Starbursts, ed. S. Huettemeister & E. Manthey (Melville: AIP), 223
Shlosman, I., Begelman, M. C., & Frank, J. 1990, Nature, 345, 679
Shlosman, I., Frank, J., & Begelman, M. C. 1989, Nature, 338, 45
Shlosman, I., & Heller, C. H. 2002, ApJ, 565, 921
Shlosman, I., & Noguchi, M. 1993, ApJ, 414, 474
Skokos, Ch., Patsis, P. A., & Athanassoula, E. 2002, MNRAS, 333, 847
Toomre, A. 1966, Notes on the Summer School Program in Geophysical Fluid Dynamics at the Woods Hole Oceanographic Institution, 66, 111
Tremaine, S., & Weinberg, M. D. 1984, MNRAS, 209, 729
Weinberg, M. D. 1985, MNRAS, 213, 451